

# Temperature-Dependent Adhesion in van der Waals Heterostructures

Jonathan M. Polfus,\* Marta Benthem Muñiz, Ayaz Ali, Daniel A. Barragan-Yani, Per Erik Vullum, Martin F. Sunding, Takashi Taniguchi, Kenji Watanabe, and Branson D. Belle\*

The interlayer coupling between 2D materials is immensely important for both the fundamental understanding of these systems, and for the development of transfer techniques for the fabrication of van der Waals (vdW) heterostructures. A number of uncertainties remain with respect to their adhesion characteristics due to the elusive nature of measured adhesion interactions. Moreover, it is theoretically predicted that the intrinsic ripples in 2D materials give rise to a temperature dependence in adhesion, although the vdW interactions themselves are principally independent of temperature. Here, direct measurements of the adhesion between reduced graphene oxide – coated by solution deposition on atomic force microscopy tips – and graphene, h-BN, and MoS<sub>2</sub> supported on SiO<sub>2</sub> substrates and as freestanding membranes are presented. The in situ nanomechanical characterization reveals a prominent reduction in the adhesion energies with increasing temperature which is ascribed to the thermally induced ripples in the 2D materials.

physical properties pave the way for a greater range of functionality in materials and devices.<sup>[3]</sup> The adhesion characteristics between 2D materials are not only of fundamental interest for understanding the bonding and properties of heterostructures, but also for the development of fabrication pathways involving transfer by vdW pickup, as well as growth mechanisms of 2D crystals.<sup>[4]</sup>


The adhesive properties of 2D materials have been studied using a variety of approaches at micro- and nanoscopic scales, addressing adhesion to metal and oxide substrates, and increasingly between 2D materials.<sup>[5–7]</sup> In particular, nanomechanical atomic force microscopy (AFM) techniques have been employed for the direct measurement of the interactions between graphene

and the tip material.<sup>[8,9]</sup> Advances in the coating of AFM tips with graphitic materials have not only led to improved wear resistance and electrical characterization,<sup>[10–14]</sup> but also the possibility for probing interlayer interactions between 2D materials. Li et al. conducted a qualitative comparison of the adhesion between a ≈10 nm graphite-wrapped AFM tip and flakes of MoS<sub>2</sub> and h-BN.<sup>[15]</sup> Using tip-attached 2D crystals, Rokni and Lu recently

## 1. Introduction

2D materials – exhibiting covalent intralayer bonding and comparatively weak interlayer coupling – can be isolated as individual layers,<sup>[1]</sup> and consequently, stacked into artificial van der Waals (vdW) heterostructures.<sup>[2]</sup> As originally envisioned by Feynman, heterostructures comprising layers with distinct

J. M. Polfus,<sup>[†]</sup> M. B. Muñiz,<sup>[††]</sup> M. F. Sunding, B. D. Belle  
Department of Sustainable Energy Technology  
SINTEF  
Forskingsveien 1, Oslo 0373, Norway  
E-mail: jonathan.polfus@kjemi.uio.no; branson.belle@sintef.no  
A. Ali  
Department of Smart Sensor Systems  
SINTEF DIGITAL  
Forskingsveien 1, Oslo 0373, Norway

 The ORCID identification number(s) for the author(s) of this article can be found under <https://doi.org/10.1002/admi.202100838>.

© 2021 The Authors. Advanced Materials Interfaces published by Wiley-VCH GmbH. This is an open access article under the terms of the Creative Commons Attribution License, which permits use, distribution and reproduction in any medium, provided the original work is properly cited.

<sup>[†]</sup>Present address: Department of Chemistry, Centre for Materials Science and Nanotechnology, University of Oslo, POB 1033 Blindern, NO-0315 Oslo, Norway

<sup>[††]</sup>Laboratory of Physics of Complex Matter, Ecole Polytechnique Fédérale de Lausanne (EPFL), 1015 Lausanne, Switzerland

DOI: 10.1002/admi.202100838

A. Ali  
Department of Electronic Engineering  
University of Sindh  
Jamshoro 76080, Pakistan  
D. A. Barragan-Yani  
Department of Physics and Materials Science  
University of Luxembourg  
Luxembourg L-1511, Luxembourg  
P. E. Vullum  
Department of Materials and Nanotechnology  
SINTEF  
Høgskoleringen 5, Trondheim 7034, Norway  
T. Taniguchi  
International Center for Materials Nanoarchitectonics  
National Institute for Materials Science  
1-1 Namiki, Tsukuba 305-0044, Japan  
K. Watanabe  
Research Center for Functional Materials  
National Institute for Materials Science  
1-1 Namiki, Tsukuba 305-0044, Japan

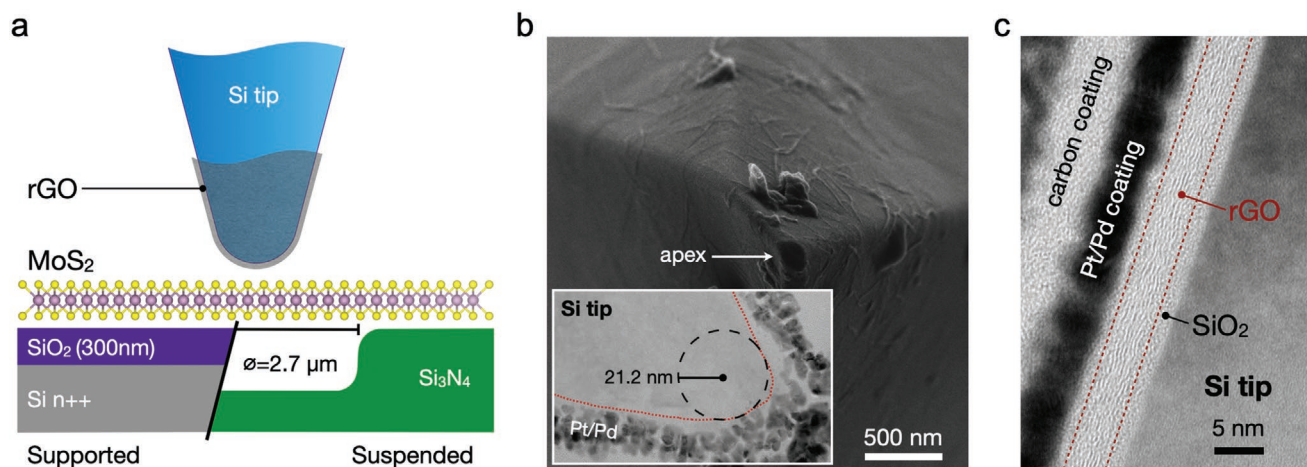


**Figure 1.** Characterization of rGO-coated AFM tip. a) Schematic overview of the AFM adhesion experiments exemplified with MoS<sub>2</sub>. b) SEM image of AFM tip (top view) with the rGO coating visible as fringes, and some debris/particles determined not to influence adhesion measurements. Inset: TEM bright field image of the tip apex (cross-section) showing the outline of the tip and the spherical tip radius as determined from AFM calibration. c) TEM bright field image of the rGO coating on the AFM tip encapsulated by Pt/Pd and carbon protection layers. All images were acquired after the adhesion measurements.

reported adhesion energies between multilayer graphene, h-BN, and MoS<sub>2</sub>, with focus on the role of annealing and contaminants in ambient air.<sup>[16]</sup>

Interlayer adhesion energies between graphene and/or graphite have been reported in the range of 0.22–0.31 J m<sup>-2</sup>.<sup>[5,17]</sup> However, there are significant discrepancies in adhesion energies obtained by different approaches, in particular for vdW heterostructures.<sup>[7]</sup> For instance, adhesion energies of 0.13–0.14 J m<sup>-2</sup> were reported for heterostructures of graphene and h-BN or MoS<sub>2</sub> based on height profiles of spontaneously formed blisters,<sup>[18]</sup> while values of 0.25–0.30 J m<sup>-2</sup>, seemingly independent of the 2D material, were obtained based on an AFM technique.<sup>[16]</sup> The nature of measured adhesion energies remains elusive in many cases due to potential extrinsic contributions from chemical and capillary forces associated with the presence of humidity and hydrocarbons in the ambient atmosphere,<sup>[16,19]</sup> as well as residue from sample preparation. In this respect, chemisorbed water can be particularly difficult to remove, and bridging chemical bonds may form between reduced graphene oxide (rGO) and oxide substrates.<sup>[20]</sup> Water may also be confined in between the substrate and 2D crystal, even after degassing at 650 °C in ultra-high vacuum.<sup>[21]</sup> Another effect of temperature on adhesion can arise from differences in the thermal expansion of the interfacing materials.<sup>[22]</sup> Specifically for AFM-based approaches, it is particularly challenging to accurately account for the role of a water meniscus at the tip apex due to the complex relationship between the capillary forces and tip characteristics, as well as the dynamics of meniscus formation.<sup>[23]</sup> Graphene-coated AFM tips thus show additional benefits due to the hydrophobic nature of graphene,<sup>[14]</sup> and the measurements in the present work were additionally conducted under controlled and nominally dry atmosphere.

The noncovalent interlayer interactions, which are predominated by vdW dispersion, arise from dynamic electron correlations and are proportional to the polarizability of the interacting materials. The interlayer interactions can therefore be expected to be the largest for graphene, followed by MoS<sub>2</sub> and h-BN, representing semimetals, semiconductors, and

insulators, respectively. The interlayer interactions are in principle independent of temperature except for the minor contribution from the Keesom dipole–dipole interactions. The main impact of temperature on the adhesion may be of structural origin, and specifically related to the presence of nanoscopic ripples that are inevitable in 2D materials according to theoretical predictions.<sup>[24]</sup> These intrinsic ripples are induced by thermal vibrations at finite temperatures, as observed in freestanding graphene and MoS<sub>2</sub>,<sup>[25,26]</sup> and in supported graphene.<sup>[27]</sup> Based on statistical mechanics analysis and molecular dynamics simulations, Wang et al. predicted that the average separation between graphene and its support would increase with temperature due to nanoscopic ripples, accompanied by a decrease in the effective adhesion energy.<sup>[28]</sup> This thermal effect on the adhesive properties of 2D materials is yet to be confirmed experimentally. The present work elucidates the role of temperature on the adhesion characteristics between an rGO-coated tip with freestanding and supported 2D materials (Figure 1a), and its further implications for stacking of vdW heterostructures, given the reported discrepancies.<sup>[29,30]</sup>

## 2. Results and Discussions

The complete coating of the apex of the AFM tips with rGO was confirmed by scanning and transmission electron microscopy (SEM and TEM). The presence of rGO is evidenced by the ripples in the SEM image of the rGO-coated tips (Figure 1b). Cross-section TEM, at locations where the layers could be imaged edge on, showed that the coating exhibited a uniform thickness of ≈4 nm and consisted of 6–7 monolayers with an interlayer distance of about 4.0 Å (Figure 1c). The quality of the rGO material was ensured by Raman spectroscopy directly on the AFM cantilever (Figure S7, Supporting Information), and X-ray photoelectron spectroscopy (XPS) revealed a C:O ratio of 5.7 with epoxide as the main oxygen group (Figure S6, Supporting Information). Crucially, the rGO coating remained intact after the

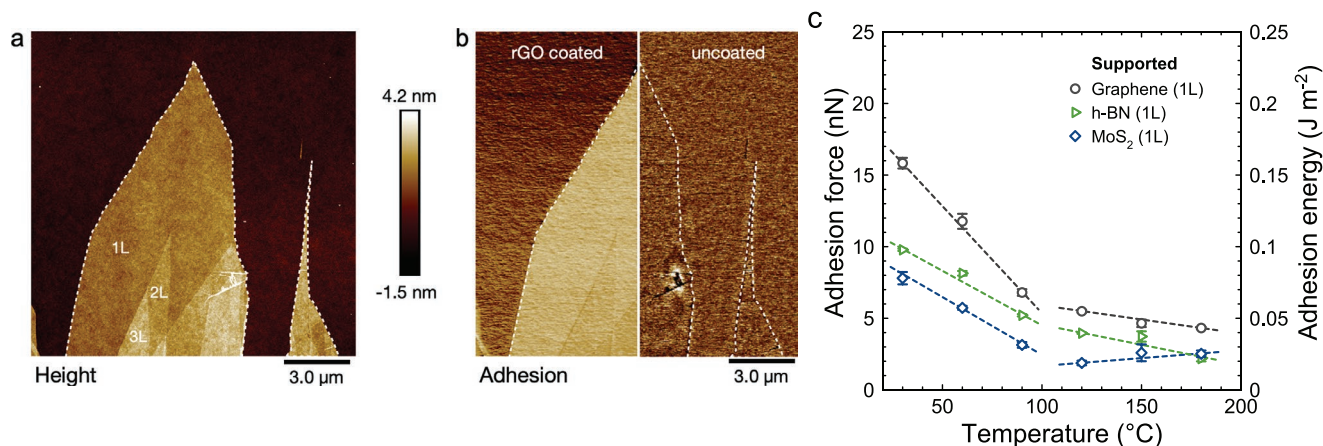


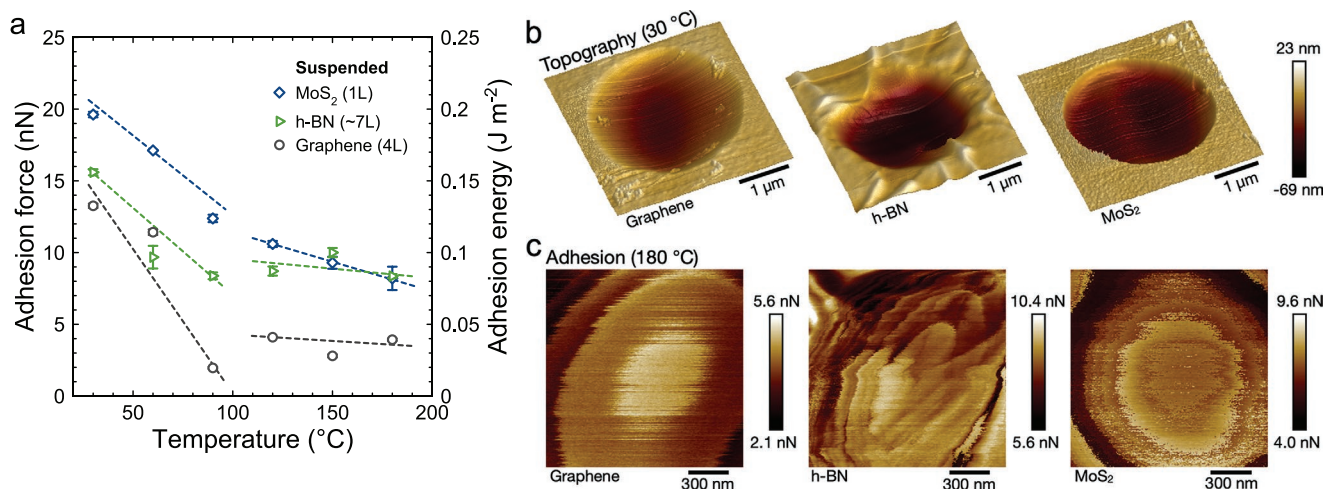
**Figure 2.** Adhesion measurements on supported samples. a) AFM topography map of graphene flakes on SiO<sub>2</sub> substrate. b) Qualitative adhesion maps of the same region using an rGO-coated (left) and uncoated (right) tip. c) Adhesion force/energy as a function of temperature between rGO-coated tip and monolayer graphene, h-BN, and MoS<sub>2</sub> supported on SiO<sub>2</sub>.

adhesion measurements and thermal cycling, demonstrating the durability of the rGO material and its adherence to the Si tip. The size and shape of the tip apex as determined from the TEM cross-section was found to be in excellent agreement with the radius obtained from AFM calibration (Figure 1b inset).

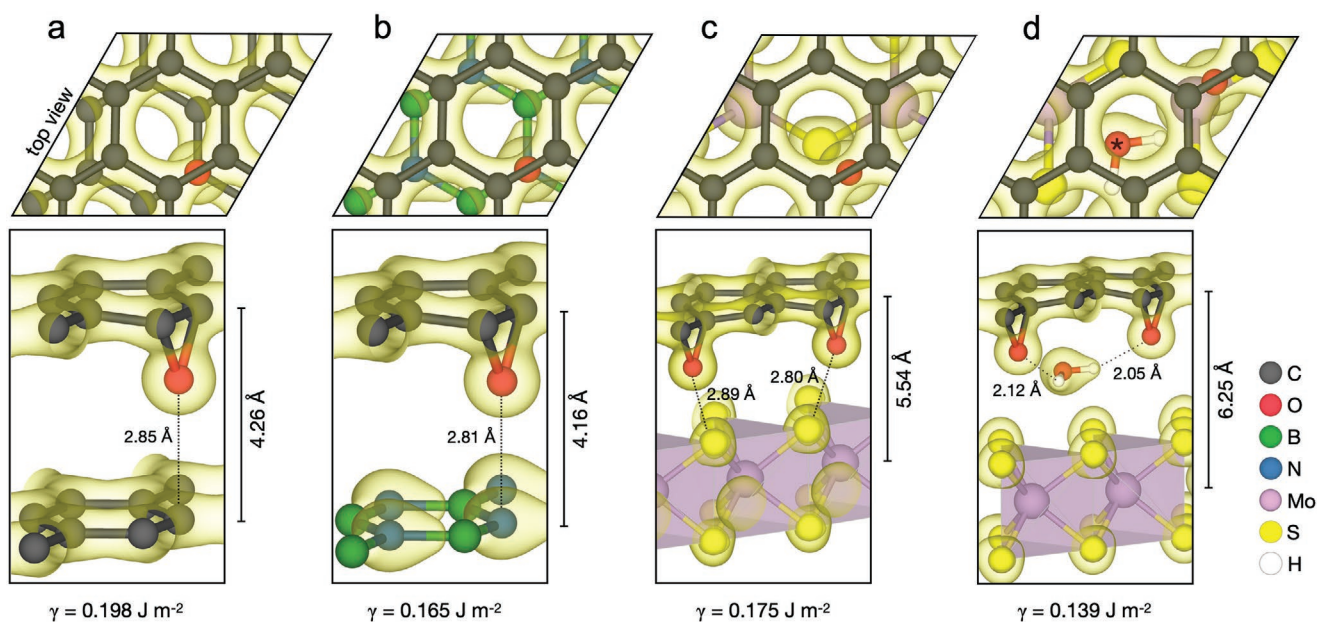
Figure 2 shows an AFM topography map of a graphene crystal supported on SiO<sub>2</sub> with mono- and multilayer regions, and the corresponding adhesion maps revealed a distinctly stronger interaction with the rGO-coated tip compared to the uncoated tip. Moreover, using the rGO-coated tip, the adhesion was higher to graphene than the SiO<sub>2</sub> substrate, while it was essentially independent of the number of graphene layers. In order to reduce the influence of water or other volatile species, quantitative adhesion measurements were performed from 180 °C to room temperature with a 30 min dwell time at each temperature in an argon atmosphere. The results are summarized for the supported monolayers in Figure 2c with the corresponding adhesion energies calculated using the Johnson–Kendall–Roberts (JKR) continuum mechanics model with tip radius and adhesion force as inputs.<sup>[31]</sup> The adhesion energies

exhibit a substantial decrease with increasing temperature, in line with the expected effect of thermal ripples. The roughness of the supported samples remained low throughout the temperature range, indicating that the ripples mainly serve to increase the average interlayer distance (Figure S10, Supporting Information). As indicated by the eye guides, there appears to be a transition at around 100 °C, and the potential influence of water impurities should be considered further. The measured adhesion to the bare SiO<sub>2</sub> substrate was approximately linear throughout the temperature range (Figure S9, Supporting Information), which may be ascribed to a reduced effect of thermal ripples in the rGO coating and/or with only one 2D material, or the higher hydrophilicity of SiO<sub>2</sub> and presence of water even up to the highest temperatures. Notably, the data points exhibited low standard deviation from five consecutive measurements, each comprising an average of a 256 × 256 pixel adhesion map.

In order to account for role of the substrate on the adhesion characteristics, freestanding membranes were prepared of graphene (4 layers), h-BN (≈7 layers), and monolayer MoS<sub>2</sub>. For these suspended membranes, the adhesion to the rGO-coated tip



**Figure 3.** Adhesion and nanomechanical characterization of suspended samples. a) Adhesion force/energy as a function of temperature between rGO-coated AFM tip and suspended graphene, h-BN, and MoS<sub>2</sub>. b, c) AFM topography maps at 30 °C and adhesion maps at 180 °C of suspended graphene (4 layers), h-BN (≈7 layers), and monolayer MoS<sub>2</sub>.



**Figure 4.** Heterostructures and adhesion energies from ab initio calculations. a) rGO and graphene with epoxide directly above carbon. b) rGO and h-BN with epoxide directly above nitrogen. c) rGO and MoS<sub>2</sub> with three out of four inequivalent epoxide groups directed toward S (two shown). d) rGO and MoS<sub>2</sub> with one interlayer H<sub>2</sub>O molecule. The C:O ratio in rGO was 8 and the charge densities are shown as 0.15 e Å<sup>-3</sup> isosurfaces.

displayed a similar behavior as the supported membranes over the whole temperature range, notably including monolayer MoS<sub>2</sub> (Figure 3). Thus, water associated with the substrate or in between layers in the membranes cannot be the main cause of the variation in adhesion with temperature. Any remaining extrinsic effects therefore appear to be limited to the presence of water impurities in between the tip and 2D material or within the rGO layers. Overall, the adhesion values were higher for the suspended membranes in comparison to the supported monolayers. The topographic maps in Figure 3b show that the membranes tended to dip into the holes to somewhat varying degrees, likely influenced by the membrane thickness and the mechanical properties of the materials. Nanomechanical characterization revealed that the suspended membranes were softer than the supported monolayers, as exemplified by the dissipation maps (Figure S11, Supporting Information). Consequently, the suspended membranes can be expected to conform to the shape of the tip and thereby lead to larger effective interaction areas and higher adhesion values. While the adhesion characteristics of the suspended membranes provide important insight into the role of substrate, temperature, and impurities, reliable adhesion energies were for these reasons difficult to extract. The topographic and adhesion maps of the membranes displayed concentric rings consistent with large ripples with wavelengths >100 nm (Figure 3c and Figure S12 (Supporting Information)).<sup>[24]</sup> The roughness of the suspended membranes showed a slight tendency to increase with increasing temperature (Figure S10, Supporting Information). Thermal expansion of the membrane relative to the support may also contribute to the formation of these types of ripples or wrinkles.<sup>[22]</sup>

In order to assess the theoretical magnitude and nature of the adhesive interactions in the rGO-based heterostructures, ab initio atomistic modeling was performed using state-of-the-art vdW density functionals that have been shown to provide accurate adhesion energies and interlayer distances in 2D materials.<sup>[32]</sup>

The calculated adhesion energies may be considered to represent an upper bound compared to the experiments due to the atomically flat and commensurate heterostructures in the periodic computational cells. In line with the XPS characterization, rGO was modeled with epoxide as the main oxygen group and C:O ratios of 8 and 5.3.<sup>[20]</sup> The optimized heterostructures are illustrated with charge density isosurfaces in Figure 4 together with the corresponding adhesion energies and averaged interlayer distances. In these most stable configurations, the epoxide groups were positioned directly above or close to the regions of highest electron density in the heterostructures, i.e., carbon, nitrogen, and sulfur in graphene, h-BN, and MoS<sub>2</sub>, respectively, at distances of 2.8–2.9 Å. Nevertheless, the variation in adhesion energy between configurations with different lateral positions of the epoxide group was determined to be minor, i.e., within 0.01 J m<sup>-2</sup>, in line with the nonlocality of the vdW interactions. The obtained adhesion energies followed the same trend as expected from the polarizability of the materials and amounted to 0.20, 0.18, and 0.17 J m<sup>-2</sup> for the heterostructures with graphene, MoS<sub>2</sub>, and h-BN, respectively.

The influence of interlayer H<sub>2</sub>O on the structure and adhesion energy was investigated in the case of the rGO–MoS<sub>2</sub> heterostructure. Concurrently, with an increase in interlayer distance by about 0.7 Å, insertion of a H<sub>2</sub>O molecule led to formation of relative strong hydrogen bonds between H<sub>2</sub>O and the epoxide groups in rGO (Figure 4d). Moreover, the oxygen in H<sub>2</sub>O – and its associated electron density – was closer to MoS<sub>2</sub> than the epoxide groups were in the pristine heterostructure. The adhesion energy showed a slight increase to about 0.19 J m<sup>-2</sup> with H<sub>2</sub>O, while it was reduced to about 0.14 J m<sup>-2</sup> if H<sub>2</sub>O was considered to be bound to rGO when the layers were separated. Due to the relatively strong bonding between H<sub>2</sub>O and rGO, the latter case is considered the most relevant, especially at lower temperatures. In other words, these considerations indicate that the presence of H<sub>2</sub>O would lead to stronger adhesion

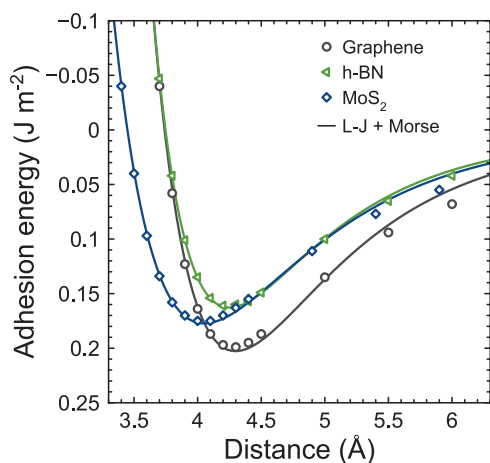


**Figure 5.** Adhesion energy as a function of distance to rGO from ab initio calculations. In the case of MoS<sub>2</sub>, the distance is measured to the sulfur layer, and the interlayer distance is obtained by adding  $d_{\text{Mo-S}} = 1.52$  Å. Lines are fits according to a combination of Lennard–Jones (L–J) and Morse potentials.

with increasing temperature and the presence of water impurities can therefore not explain the experimental observations.

The direct comparison of the calculated adhesion energies with the AFM measurements of the supported samples is enabled by the screening of the substrate by monolayer graphene or MoS<sub>2</sub>.<sup>[33,34]</sup> Due to the dielectric properties of h-BN, the adhesion measurements must be considered to include contributions for the SiO<sub>2</sub> support, which thereby may account for the higher adhesion energies obtained experimentally for h-BN than MoS<sub>2</sub> compared to the theoretical values. The measured adhesion energies at 30 °C were about 0.16 J m<sup>-2</sup> for rGO–graphene, slightly lower than the calculated value of 0.20 J m<sup>-2</sup>, and 0.08 J m<sup>-2</sup> for rGO–MoS<sub>2</sub> which was considerably lower than the calculated value of 0.18 J m<sup>-2</sup>.

The theoretical interaction profiles were probed by variation of the interlayer distance in the heterostructures. The rGO-based heterostructures display the characteristic asymptotic behavior of the attractive long-range vdW dispersion (Figure 5). The adhesion energies are reduced to about half of their equilibrium value by increasing the separation between the layers by only 1 Å. The pronounced effect of intrinsic ripples is clearly substantiated by considering that typical amplitudes of the ripples are in the order of several angstroms to nanometers for suspended samples, and somewhat damped for supported crystals due to the interaction with the substrate.<sup>[25,26,35,36]</sup> The amplitudes increase with temperature due to thermal excitation of the vibrations, but also saturate at elevated temperatures, e.g., from 0.6 Å at room temperature to about 90% of the saturation level of 1 Å at 200 °C for freestanding graphene.<sup>[37]</sup> Saturation of the ripple amplitude may therefore explain the plateau observed in the adhesion measurements at around 90–120 °C.

### 3. Conclusions

In conclusion, the present work demonstrates a pronounced decrease in adhesion with increasing temperature in 2D

materials and vdW heterostructures, which may be ascribed to variation in the effective contact area due to intrinsic ripples. The current results have important implications for the design of fabrication processes for stacking of vdW heterostructures.

### 4. Experimental Section

**Material Sample Preparation:** Samples of mono- and multilayer graphene (NGS Trading & Consulting GmbH), 2H-MoS<sub>2</sub> (2dsemiconductors.com), and h-BN were prepared by mechanical exfoliation of the corresponding bulk materials onto SiO<sub>2</sub> substrates and transferred using a dry transfer technique<sup>[29]</sup> to Si<sub>3</sub>N<sub>4</sub> prepatterned with holes of diameter 2.7 μm.

**AFM Tip Coating and Measurements:** AFM tips (NanoAndMore GmbH, SD-R30-FM-10) were dipped into a GO water dispersion (Abalonyx AS) for 1 min followed by drying at 50 °C.<sup>[14]</sup> The GO-coated tips were then reduced under flowing 5% H<sub>2</sub> in Ar for 2 h at 250 °C. Adhesion forces were measured using quantitative nanomechanical mapping (QNM) in peak-force tapping mode on a Bruker Multimode 8 with a heater/cooler J scanner. A gas cell with flowing Ar (99.9999%) was used to ensure dry measurement conditions. Prior to QNM imaging at each temperature, the spring constant for the tip was calibrated. The measurement area was  $\approx 2 \times 2$  μm for the supported samples and  $\approx 1.5 \times 1.5$  μm for the suspended samples, i.e., within the circular suspended region of diameter 2.7 μm.

**AFM Tip Characterization:** SEM imaging and TEM sample preparation were performed with a Helios G4 UX dual-beam focused ion beam (FIB). In order to distinguish the rGO coating from carbon in the protection layers deposited in the FIB, a thin layer of Pt/Pd was sputter coated onto the sample prior to FIB sample preparation. During sample preparation, coarse thinning was performed at an ion-beam acceleration voltage of 30 kV, and final thinning was performed at 5 and 2 kV on either side of the lamellae to minimize surface damage. TEM was performed with a double Cs aberration corrected cold FEG JEOL ARM 200FC, operated at 200 kV.

**Ab Initio Calculations:** Density functional theory calculations were performed using the SCAN+rVV10 vdW functional as implemented in Vienna Ab initio simulation package (VASP).<sup>[32]</sup> For the heterostructures, rGO was constructed as a 2 × 2 graphene cells with C:O ratios of 8 and 5.3 due to epoxide groups<sup>[20]</sup> and stacked together with 2 × 2 cells of graphene or h-BN, while 2 × 2 rGO cells were stacked together with 3 × 3 MoS<sub>2</sub> cells. The *k*-point grids were 16 × 16 × 1, 20 × 20 × 1, and 10 × 10 × 1 for the heterostructures of rGO and graphene, h-BN and MoS<sub>2</sub>, respectively. Adhesion energies were obtained from the total energies of heterostructures with optimized interlayer distance and atomic positions, using as reference the energy of the system with the monolayers separated by 15 Å, thereby avoiding effects of the strain.

### Supporting Information

Supporting Information is available from the Wiley Online Library or from the author.

### Acknowledgements

The authors acknowledge financial support from the Research Council of Norway (RCN) through 2Defect (Grant No. 262274) under the FRIPRO program and 2Dsense (Grant No. 280788) under the INDNOR program. RCN is also acknowledged for support to the Norwegian Micro- and Nano-Fabrication Facility (NorFab, Grant No. 295864), the NORTEM infrastructure (Grant No. 197405), and for computational resources through Uninett Sigma2 (Grant No. NN9259K). K.W. and T.T. acknowledge support from the Elemental Strategy Initiative conducted

by MEXT (Grant No. JPMXP0112101001), JSPS KAKENHI (Grant No. JP20H00354), and JST CREST (Grant No. JPMJCR15F3).

## Conflict of Interest

The authors declare no conflict of interest.

## Data Availability Statement

The data that support the findings of this study are available from the corresponding author upon reasonable request.

## Keywords

2D materials, adhesion energy, atomic force microscopy, van der Waals transfer

Received: May 25, 2021

Revised: August 30, 2021

Published online: September 27, 2021

- [1] K. S. Novoselov, A. K. Geim, S. V. Morozov, D. Jiang, Y. Zhang, S. V. Dubonos, I. V. Grigorieva, A. A. Firsov, *Science* **2004**, 306, 666.
- [2] Y. Liu, N. O. Weiss, X. Duan, H.-C. Cheng, Y. Huang, X. Duan, *Nat. Rev. Mater.* **2016**, 1, 16042.
- [3] R. P. Feynman, *Eng. Sci.* **1960**, 23, 22.
- [4] R. Frisenda, E. Navarro-Moratalla, P. Gant, D. P. De Lara, P. Jarillo-Herrero, R. V. Gorbachev, A. Castellanos-Gomez, *Chem. Soc. Rev.* **2018**, 47, 53.
- [5] J. Wang, D. C. Sorescu, S. Jeon, A. Belianinov, S. V. Kalinin, A. P. Baddorf, P. Maksymovych, *Nat. Commun.* **2016**, 7, 13263.
- [6] S. P. Koenig, N. G. Boddeti, M. L. Dunn, J. S. Bunch, *Nat. Nanotechnol.* **2011**, 6, 543.
- [7] D. Akinwande, C. J. Brennan, J. S. Bunch, P. Egberts, J. R. Felts, H. Gao, R. Huang, J.-S. Kim, T. Li, Y. Li, *Extreme Mech. Lett.* **2017**, 13, 42.
- [8] T. Jiang, Y. Zhu, *Nanoscale* **2015**, 7, 10760.
- [9] J. W. Suk, S. R. Na, R. J. Stromberg, D. Stauffer, J. Lee, R. S. Ruoff, K. M. Liechti, *Carbon* **2016**, 103, 63.
- [10] Y. Wen, J. Chen, Y. Guo, B. Wu, G. Yu, Y. Liu, *Adv. Mater.* **2012**, 24, 3482.
- [11] W. Shim, K. A. Brown, X. Zhou, B. Rasin, X. Liao, C. A. Mirkin, *Proc. Natl. Acad. Sci. USA* **2012**, 109, 18312.
- [12] M. Lanza, A. Bayerl, T. Gao, M. Porti, M. Nafria, G. Jing, Y. Zhang, Z. Liu, H. Duan, *Adv. Mater.* **2013**, 25, 1440.
- [13] C. Martin-Olmos, H. I. Rasool, B. H. Weiller, J. K. Gimzewski, *ACS Nano* **2013**, 7, 4164.
- [14] F. Hui, P. Vajha, Y. Shi, Y. Ji, H. Duan, A. Padovani, L. Larcher, X. R. Li, J. J. Xu, M. Lanza, *Nanoscale* **2016**, 8, 8466.
- [15] B. Li, J. Yin, X. Liu, H. Wu, J. Li, X. Li, W. Guo, *Nat. Nanotechnol.* **2019**, 14, 567.
- [16] H. Rokni, W. Lu, *Nat. Commun.* **2020**, 11, 5607.
- [17] P. Li, Z. You, T. Cui, *Sens. Actuators, A* **2014**, 217, 56.
- [18] D. A. Sanchez, Z. Dai, P. Wang, A. Cantu-Chavez, C. J. Brennan, R. Huang, N. Lu, *Proc. Natl. Acad. Sci. USA* **2018**, 115, 7884.
- [19] E. Khestanova, F. Guinea, L. Fumagalli, A. Geim, I. Grigorieva, *Nat. Commun.* **2016**, 7, 12587.
- [20] J. M. Polfus, K. Jayasayee, *Carbon* **2019**, 152, 497.
- [21] K. T. He, J. D. Wood, G. P. Doidge, E. Pop, J. W. Lyding, *Nano Lett.* **2012**, 12, 2665.
- [22] Y. He, W. Yu, G. Ouyang, *J. Phys. Chem. C* **2015**, 119, 5420.
- [23] A. J. Harrison, D. S. Corti, S. P. Beaudoin, *Part. Sci. Technol.* **2015**, 33, 526.
- [24] S. Deng, V. Berry, *Mater. Today* **2016**, 19, 197.
- [25] J. C. Meyer, A. K. Geim, M. I. Katsnelson, K. S. Novoselov, T. J. Booth, S. Roth, *Nature* **2007**, 446, 60.
- [26] J. Brivio, D. T. Alexander, A. Kis, *Nano Lett.* **2011**, 11, 5148.
- [27] M. Ishigami, J. Chen, W. Cullen, M. Fuhrer, E. Williams, *Nano Lett.* **2007**, 7, 1643.
- [28] P. Wang, W. Gao, R. Huang, *J. Appl. Phys.* **2016**, 119, 074305.
- [29] C. R. Dean, A. F. Young, I. Meric, C. Lee, L. Wang, S. Sorgenfrei, K. Watanabe, T. Taniguchi, P. Kim, K. L. Shepard, *Nat. Nanotechnol.* **2010**, 5, 722.
- [30] A. Kretinin, Y. Cao, J. Tu, G. Yu, R. Jalil, K. Novoselov, S. Haigh, A. Gholinia, A. Mishchenko, M. Lozada, *Nano Lett.* **2014**, 14, 3270.
- [31] K. L. Johnson, K. Kendall, A. D. Roberst, *Proc. R. Soc. London, Ser. A* **1971**, 324, 301.
- [32] H. Peng, Z.-H. Yang, J. P. Perdew, J. Sun, *Phys. Rev. X* **2016**, 6, 041005.
- [33] S. Tsoi, P. Dev, A. L. Friedman, R. Stine, J. T. Robinson, T. L. Reinecke, P. E. Sheehan, *ACS Nano* **2014**, 8, 12410.
- [34] A. Gurarlan, S. Jiao, T. D. Li, G. Li, Y. Yu, Y. Gao, E. Riedo, Z. Xu, L. Cao, *Adv. Mater.* **2016**, 28, 10055.
- [35] P. Miró, M. Ghorbani-Asl, T. Heine, *Adv. Mater.* **2013**, 25, 5473.
- [36] Z. Chang, R. Yang, Y. Wei, *J. Mech. Phys. Solids* **2019**, 132, 103697.
- [37] S. M. Mofidi, H. Nejat Pishkenari, M. R. Ejtehad, A. V. Akimov, *J. Phys. Chem. C* **2019**, 123, 20026.